IOP Conf. Series: Materials Science and Engineering **142** (2016) 012072 doi:10.1088/1757-899X/142/1/012072

Influence of Material Models Used in Finite Element Modeling on Cutting Forces in Machining

Vusal Jivishov, Elchin Rzayev

Azerbaijan Technical University.
H. Javid pr. 25, Az 1073, Baku, Azerbaijan

E-mail: elchin_rz@mail.ru

Abstract. Finite element modeling of machining is significantly influenced by various modeling input parameters such as boundary conditions, mesh size and distribution, as well as properties of workpiece and tool materials. The flow stress model of the workpiece material is the most critical input parameter. However, it is very difficult to obtain experimental values under the same conditions as in machining operations.. This paper analyses the influence of different material models for two steels (AISI 1045 and hardened AISI 52100) in finite element modelling of cutting forces. In this study, the machining process is scaled by a constant ratio of the variable depth of cut h and cutting edge radius rß. The simulation results are compared with experimental measurements. This comparison illustrates some of the capabilities and limitations of FEM modelling.

Introduction

With the rapid increase of computing performance in the last two decades, finite element modeling of the machining process became possible and can be conducted with minimal costs. Finite element methods are appropriate tools for predicting variables such as stresses, strains, temperatures and cutting forces during the machining process. However, these predicted variables are significantly influenced by the simulation input parameters and boundary conditions. The most significant input parameter for the simulation are the material flow stress data, also known as material model. Several researchers studied the discrepancies of different material models for the same material and found out that it has a great influence on the predicted variables in machining [1, 2, 3].

This paper investigates the influence of material model on the modeling of cutting forces. The investigations taking place by a constant ratio of cutting edge radius $r_ß$ to depth of cut h. The experiments are carried out using two different steels, AISI 1045 (Ck45) and hardened AISI 52100 (100Cr6), as workpiece material. Uncoated carbide cutting tools with edge radii of 0.01 mm and 0.5 mm are used to cut the AISI 1045 workpiece and CBN cutting tools with edge radii of 0.008°mm and 0.12 mm are used to cut the hardened AISI 52100. The predictions are compared with cutting forces obtained from orthogonal cutting experiments conducted with the same materials and cutting conditions. The edge radii of all of the cutting tools that are used in the experiments are measured preliminary.

DEFORM-2D®, a commercial finite element code that has been validated for cutting simulations [15], is used for the simulations. In this study orthogonal cutting experiments are represented with plane strain model since no side flow was observed. To achieve simulation models close to the reality, large and small workpieces were used. Furthermore small sized mesh elements are used in the simulations especially near the tools' edges (less than 0.001 mm for smaller depth of cut h). This cutting model is used for the simulations using the different material models of each steel for the respective cutting conditions.

Material Models for AISI 1045

Four material models of AISI 1045 are compared in this study, Johnson–Cook [4], Koppka [5], El-Magd [6] and Oxley [7]. The mentioned material models are determined using compression tests, except for the Koppka model. Koppka's model is based on flow stress data obtained from machining tests, and thereupon the Johnson-Cook's equation was modified. All material models are compared using their behavior at averaged values of strain, strain rate and temperature. The cutting forces and chip morphology are obtained from cutting simulation and experiment.

Johnson-Cook's model:

$$\sigma = \left[A + B\left(\varepsilon_p\right)^n\right]\left[1 + C\ln\left(\frac{\dot{\varepsilon}_p}{\dot{\varepsilon}_0}\right)\right]\left(1 - \theta^m\right) \qquad [1]$$

El-Magd's model:

$$\sigma\left(\varepsilon, \dot{\varepsilon}, T\right) = \left(K\left(B + \varepsilon\right)^n + \eta\dot{\varepsilon}\right)\exp\left[-\beta_1 \frac{T - T_0}{T_m}\right] \quad [2]$$

Oxley and co-workers used the velocity modified temperature concept to describe material properties as a function of strain rate and temperature.

$$\sigma = \sigma_1 \varepsilon^n \text{ where } n = f\left(T_{mod}\right) \qquad [3]$$

Thereby T_{mod} is calculated as follows

$$T_{mod} = T\left[1 - \nu\log\left(\frac{\dot{\varepsilon}}{\dot{\varepsilon}_0}\right)\right] \text{ where } \nu = 0.09 \text{ and } \dot{\varepsilon}_0 = 1 \qquad [4]$$

increases as the temperature increases and decreases as the strain rate increases. T and $\dot{\varepsilon}$ describe the testing temperature and strain rate, and ν and $\dot{\varepsilon}_0$ are material constants for a given material and a range of testing conditions

Koppka's model:

$$\sigma = \left[B\varepsilon^n\right]\left[1 + C\ln\left(\frac{\dot{\varepsilon}}{1000}\right)\right]\left[T^* + ae^{-0.00005\left(T-700\right)^2}\right] \qquad [5]$$

where

$$T^* = \left[\frac{T_{melt} - T}{T_{melt} - T_{room}}\right]$$

Tab. 1 shows the different constants for the material model equations. The Oxley model does not have any constants.

Tab. 1: Constants for Material Models (AISI 1045).

Johnson-Cook	A = 316 MPa; B = 1067 MPa; n = 0.107; C = 0.0277; m = 0,7
El-Magd	K = 1341 MPa; B = 0; n = 0.17; η = 0.02 MPa·s; β_1 = 1,5; T_m = 1808 K
Koppka	B = 996.1 MPa; n = 0.168; C = 0.097; a = 0.275; T_{melt} = 1480 ºC

For the analyses, the flow stress curves of the studied material models for AISI 1045 are compared at the same conditions of strain, strain rate, and temperature. The used constants are defined in tab 1. Fig. 1 illustrates a comparison of true stress-temperature curves at constant values of strain (1 mm/mm) and strain rate (3000 1/sec) that are estimated from simulation. The figure shows that all curves obtained from the different models except Koppka's are located within a range and slope up to a temperature of 400 ºC. At higher temperatures, Oxley's and Koppka's models have large shape deviations compared to the other models. Fig. 2 illustrates true stress versus true strain at a temperature of 250 ºC and at a strain rate of 3000 1/sec. The figure shows that all material models differ at a temperature of 250 ºC and a strain rate of 3000 1/sec. Fig. 3 shows true stress versus strain rate at a temperature of 20 ºC and at a strain of 1. It is shown clearly that the material behavior based on the El-Magd model is different from the other models at very high strain rates (> 104 /sec).

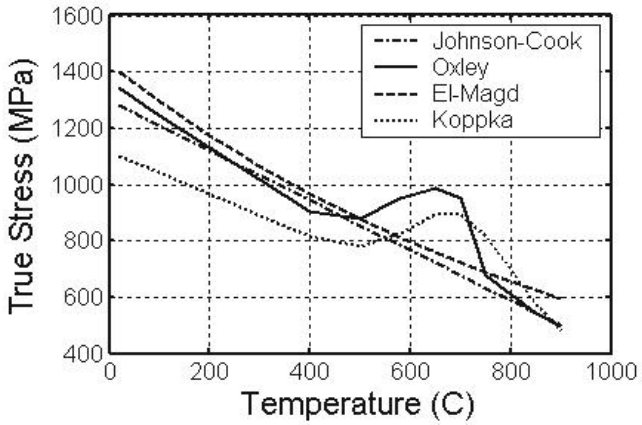

Fig. 1: Stress versus Temperature at True Strain=1 and Strain Rate=3000/sec (AISI 1045)

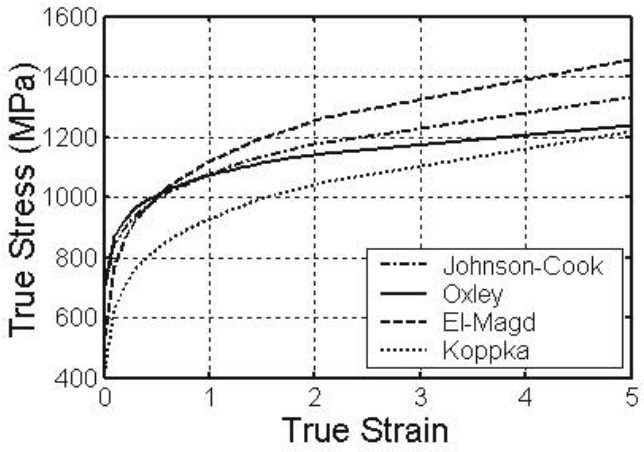

Fig. 2: Stress versus Strain at Temperature=250 °C and Strain Rate=3000/sec (AISI 1045)

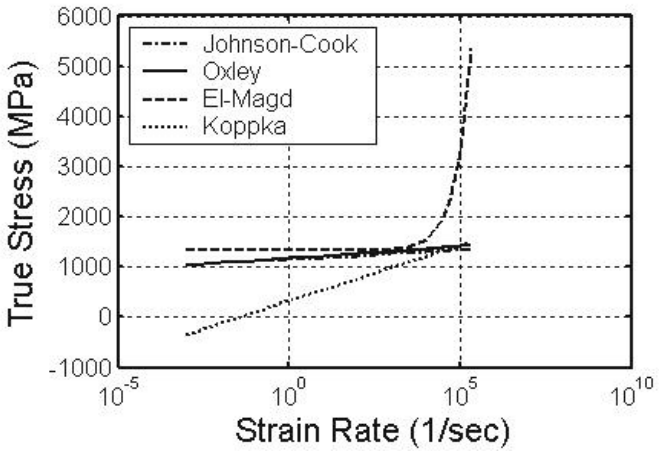

Fig. 3: Stress versus Strain Rate at Strain=1 and Temperature=20° C (AISI 1045)

Although all the models are for the same material there are significant variations between each model. This difference can influence the output variables from machining simulation.

Material Models for AISI 52100

There are several material models for AISI 52100 available in the literature [8-13]. Four different material models of hardened AISI 52100 are considered in this study. The Poulachon model [8], the Poulachon-IEP model with the same equation as the one used by Poulachon but with experimental constants obtained by IEP (Institut of experimenthal Physics, Universty of Magdeburg) [9], the Huang model [11], and Huang's model coupled with Umbrello's model [12]. The equations used in each model are listed below with constants illustrated in tab. 2.

Poulachon's model and Poulachon-IEP's model:

$$\sigma = (\mathrm{A} + \mathrm{B}\varepsilon^{-\mathrm{n}})(1 - \mathrm{CT}) \qquad [6]$$

Huang's model:

$$\sigma = (\mathrm{A} + \mathrm{B}\varepsilon^{\mathrm{n}}) \cdot (1 + \mathrm{C} \cdot \ln \dot{\varepsilon}) \left| 1 - \left(\frac{\mathrm{T} - 25}{1487 - 25} \right)^{\mathrm{m}} \right| \qquad [7]$$

Umbrello's model:

$$\sigma = B(T)(C\varepsilon^{n} + F + G\varepsilon)[1 + (\ln(\dot{\varepsilon})^{m} - A] \qquad [8]$$

where

$$F(HRC) = 27.4HRC - 1700.2 \qquad [9]$$

$$G(HRC) = 4.48HRC - 279.9 \qquad [10]$$

Huang's and Umbrello's models are coupled so that the material behaviour at the primary shear zone is represented by Huang's model and the deformation on the remaining workpiece body is represented by Umbrello's model. The flow stress coupled model proved to give better predictions for cutting forces and chip formation compared to orthogonal cutting experiments [14].

Tab. 2 shows the constants of the various material models of AISI 52100.

Poulachon	A = 11.032 MPa; B = 4783 MPa; n = 0.0946; C = 0,00129
Poulachon-IEP	A = 2000 MPa; B = 1600 MPa; n = 0.2; C = 0.0173
Huang	A = 774.78 MPa; B = 134.46 MPa; n = 0.3710; C = 0.0173; m = 3.171
Umbrello	A = 0.0567; n = 0.083; C = 1092 MPa; m = 0.1259

A similar approach to the one used for comparing the various AISI 1045 material models is used for comparing hardened AISI 52100 material models. Fig. 4 shows true stress versus temperature curves at a strain of 1 and at a strain rate of 3000 1/sec.

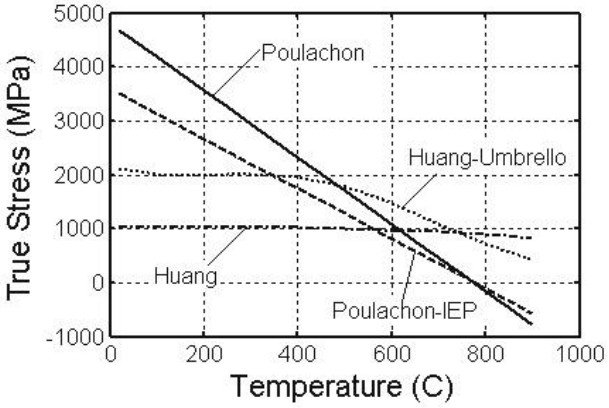

Fig. 4: Stress versus Temperature at True Strain=1 and Strain Rate=3000/sec (AISI 52100)

The curves generated from the presented material models are different. At room temperature, Poulachon's model has the highest value of true stress and Huang's model has the lowest true stress value. In addition, Huang's model is less sensitive to the increase of temperature. Fig. 5 shows true stress versus true strain curves at a temperature of 250 ºC and a strain rate of 3000 1/sec. Poulachon's model gives the highest level of true stress and Huang's model gives the lowest, corresponding to what is observed on fig. 4. Finally fig. 6 illustrates a comparison of true stress versus strain rate curves at fixed values of strain and temperature. The figure shows that the Poulachon and Poulachon-IEP models are not dependent on strain rate, whereas the flow stress value based on Huang's and Huang-Umbrello's models increases with the increase of strain rate.

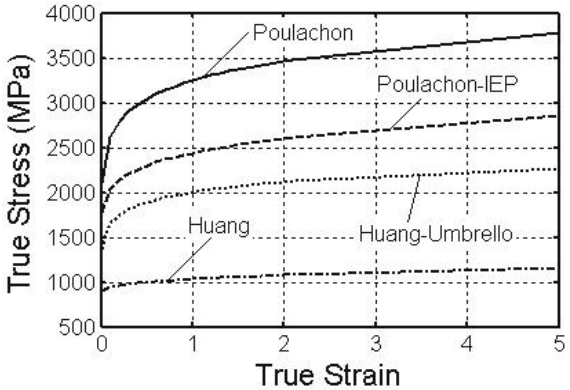

Fig. 5: Stress versus Strain at Temperature=250 °C and Strain Rate=3000/sec (AISI 52100)

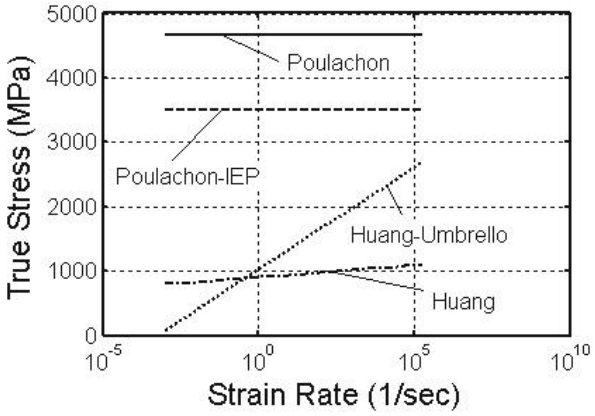

Fig. 6: Stress versus Strain Rate at Strain=1 and Temperature=20° C (AISI 52100)

Results

The cutting conditions used in simulation are identical to those of the experimental investigations. The results show that the influence of material models on cutting forces is significant. In fig. 7 a comparison of the cutting forces obtained from cutting AISI 1045 by a constant ratio of r_β / h = 1 and at a depth of cut h = 0.01 mm is shown. The cutting forces predicted using Oxley's material model are closer to the measured forces then the forces predicted using Koppka's model, the highest error occurs when using El-Magd's model.

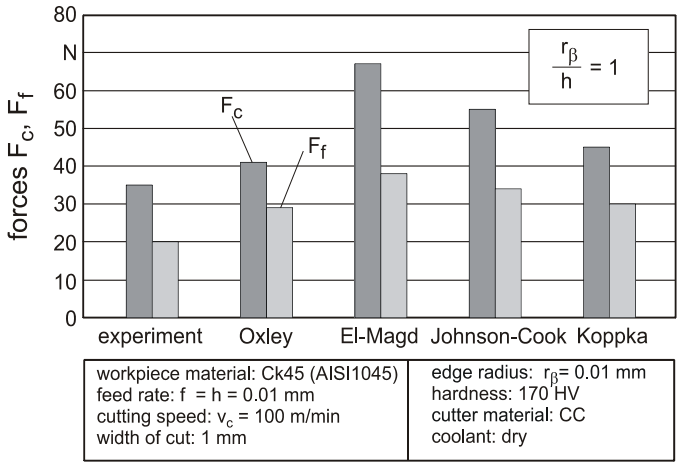

Fig. 7: Forces of AISI 1045 by smaller depth of cut h

Fig. 8 illustrates the cutting forces that are predicted by a constant ratio of r_β / h = 1 and at a depth of cut h = 0.5 mm. In the figure, Koppka's model is adequate to the experimental force of cutting but gives smaller value for the feed force. Therefore Oxley's model is expected to give better predictions of the cutting forces. However, the cutting forces predicted using El-Magd's model are very low compared to the measured forces. In fact, the forces predicted using El-Magd's model are larger than the measured forces by a smaller depth of cut and smaller than the measured forces by a larger depth of cut.

The analysis of the forces that are generated from the various material models of AISI 1045 shows that Oxley's model gives the best predictions when cutting by a constant ratio of r_β / h = 1 and different depth of cut h.

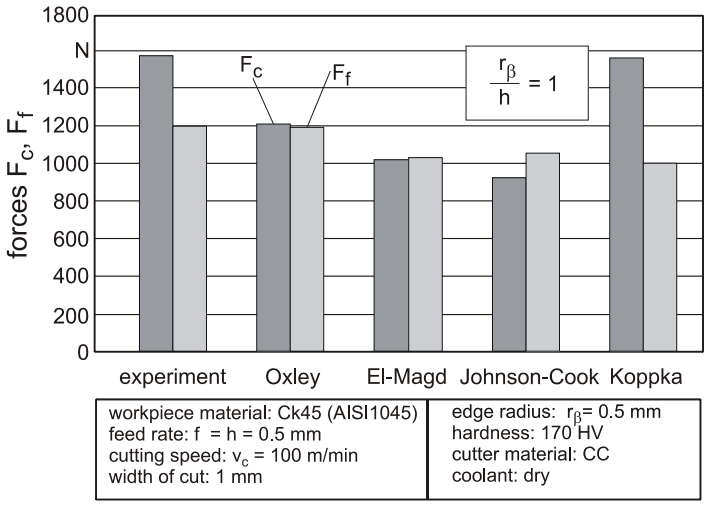

Fig. 8: Forces of AISI 1045 by larger depth of cut h

Due to the difference in hardness and material microstructure, the forces generated from cutting hardened AISI 52100 are larger than the forces generated from cutting AISI 1045. Moreover, the tendency to generate segmented chips is higher when cutting hardened AISI 52100.

Fig. 9 presents the forces obtained from the cutting of hardened AISI 52100 by a constant ratio of r_β / h = 1 and at a depth of cut h = 0.008 mm. Poulachon's and Poulachon-IEP's model lead to a good prediction of forces. Huang's model gives the lowest forces. The forces generated from the Huang-Umbrello coupled model are higher than the forces generated when Huang's model is used alone, but the forces are still very low compared to the measured forces. When comparing the forces by a constant ratio of r_β / h = 1 and at a depth of cut h = 0.12 mm, Poulachon's model also gives the better forces, as in fig. 10. In this case, the difference between Poulachon's model and Poulachon-IEP model in predicting the forces is larger than by the ratio of r_β / h = 1 and at a depth of cut h = 0.008 mm. The forces predicted using Huang's model by larger depth of cut h = 0.12 mm are as low as those by smaller depth of cut h = 0.008 mm.

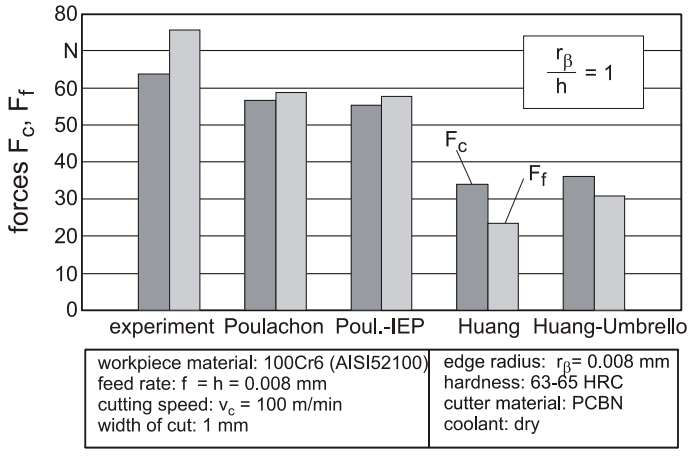

Fig. 9: Forces of AISI 52100 by smaller depth of cut h

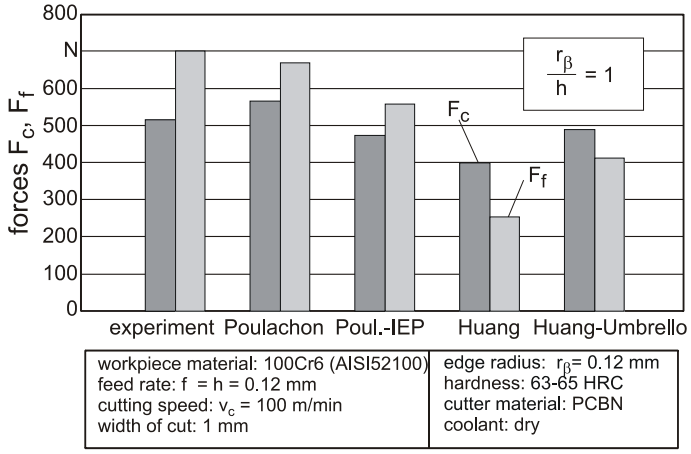

Fig. 10: Forces of AISI 52100 by larger depth of cut h

Summary and Conclusion

The results of this study show that the influence of material model on cutting forces is significant. The forces are different when different material models are used. For AISI 1045, Oxley's flow stress model leads to better results in predicting cutting forces than other models considered in this study. For AISI 52100, the Poulachon's material model shows a better prediction of cutting forces. The forces predicted using Huang-Umbrello's coupled model are much lower than the forces predicted using Poulachon's model. The results give a good understanding of how material models for the same steel are different. This leads to the conclusion that the material model may need to be validated for the specific application before the simulation takes place. Also, this observation gives more emphasis to the need for a material testing method that is capable of generating more robust material models that cover all of the material behaviour during machining.

References

[1] *Meyer, L. W.; Halle, T.; Herzig, N.:* Determination of special material behaviour and devolopment of constitutive equations for numerical simulations of high speed cutting process. Proceedings of the 8th CIRP International Workshop on Modeling of Machining, Chemnitz, Germany (2005), pp. 131-138.

[2] *Shi, J.; Liu, R.:* The Influence of Material Models on Finite Element Simulation of Machining. Journal of Manufacturing Science and Engineering, vol. 126 (2004), pp. 849-857.

[3] Adibi-Sedeh, A. H.; Vaziri, M.; Pednekar, V.; Madhavan, V.; Ivester, R.: Investigation of the Effect of Using Different Material Models on Finite Element Simulations of Machining. Proceedings of the 8th CIRP International Workshop on Modeling of Machining, Chemnitz, Germany (2005), pp. 215-224.

[4] *Johnson, R.; Cook, H.:* A Constitutive Model and Data for Metals Subjected to Large Strains, High Strain Rate, and Temperatures. International Symposium on Ballistics, The Hauge, The Netherlands (1983), pp 1-7.

[5] *Koppka, F.; Sahlan, H.; Sartkulvanich, P.; Altan, T.*: Experimental determination of flow stress data for FEM simulation of machining operations. *ERC Report,* ERC/NSM-01-R-63, 2001.

[6] *El-Magd, E; Treppmann, C.:* Mechanical Behavior of AA7075, Ck45N and TiAl6V4 at High Strain Rates. Materialsweek, Munich (2000), pp 1-8.

[7] *Oxley, P. L. B.:* The mechanics of machining: an analytical approach to assessing machinability. E. Horwood, Chichester, England, 1989.

[8] *Poulachon, G.; Moisan, A.; Jawahir, I.S.:* On modeling the influence of thermo-mechanical behavior in chip formation during hard turning of 100Cr6 bearing steel. *Annals of the CIRP*

(2001), Vol. 50, 1, pp.31-36.

[9] *Clos, R.:* Preliminary report of Project "Groesseneinfluesse beim Hartzerspanen", April, 2004

[10] *Ramesh, A.:* Prediction of process-induced microstructural changes and residual stresses in orthogonal hard machining. Ph. D. Thesis, George W. Woodruff School of Mechanical Engineering, Georgia Institute of Technology, Atlanta, Georgia, 2002.

[11] *Huang, Y.:* Predictive modeling of tool wear rate with application to CBN hard turning. Ph.D. Dissertation, The Ohio State University, Columbus, Ohio, 2002.

[12] *Umbrello, D.; Hua, J.; Shivpuri, R.:* Hardness-based flow stress and fracture models for numerical simulation of hard machining AISI 52100 bearing steel. Journal of Materials Science and Engineering (2004), Vol. A 374, pp. 90-100.

[13] *Caccialupi, A.:* Systems development for high temperature, high strain rate material testing of hard steels for plasticity behavior modeling. Master Thesis, George W. Woodruff School of Mechanical Engineering, Georgia Institute of Technology, Atlanta, Georgia, 2003.

[14] *D'Anna, L.; Al-Zkeri, I; Altan, T.:* Influence of CBN cutting tool design upon tool life and machined surface integrity, experimental and numerical investigation – verification of input data for FE modeling of hard turning. ERC/NSM Report No. HPM/ERC/NSM-05-R-38, The Ohio State University, 2005.

[15] *Yen, Y.C.; Jain, A.; Chigurupati, P.; Wu, W.T.; Altan, T.:* Computer Simulation of Orthogonal Cutting Using a Tool with Multiple Coatings. Journal of Machining Science and Technology (2004), Vol. 8, pp. 305-326.